Evidence of multimicrometric coherent γ' precipitates in a hot-forged γ-γ' nickel-based superalloy

Marie-Agathe Charpagne, Philippe Vennegues, Thomas Billot, Jean-Michel Franchet, Nathalie Bozzolo

Evidence of Multimicrometric coherent γ' precipitates in a hot-forged γ-γ' Nickel-based superalloy

Marie-Agathe Charpagne [1,2], Philippe Vennéguès [3], Thomas Billot [2], Jean-Michel Franchet [4], Nathalie Bozzolo [1]

[1] MINES ParisTech, PSL - Research University, CEMEF - Centre de mise en forme des matériaux, CNRS UMR 7635,
CS 10207 rue Claude Daunesse 06904 Sophia Antipolis Cedex, France
[2] Snecma-Safran Group, Technical Department, 171 boulevard de Valmy – BP 31, 92702 Colombes Cedex, France
[3] CRHEA-CNRS (UPR 10), Sophia Antipolis, Rue Bernard Grégory, 06560 Valbonne, France
[4] Safran SA, SafranTech – Materials & Process Department, Magny-Les-Hameaux Cedex, France

Keywords: EDS/EBSD coupling, coherent precipitates, primary precipitates, γ-γ' superalloys, lattice mismatch.

Abstract

This paper demonstrates the existence of large γ' precipitate (several micrometers in diameter) that are coherent with their surrounding matrix grain in a commercial γ-γ' Nickel-based superalloy. The use of combined EDS/EBSD (energy dispersive X-ray spectrometry and electron backscattered diffraction) analyses allowed for revealing that surprising feature, which was then confirmed by transmission electron microscopy (TEM). Coherency for such large second phase particles is supported by a very low crystal lattice misfit between the two phases, that was confirmed thanks to X-ray diffractograms and TEM selected area electron diffraction patterns.

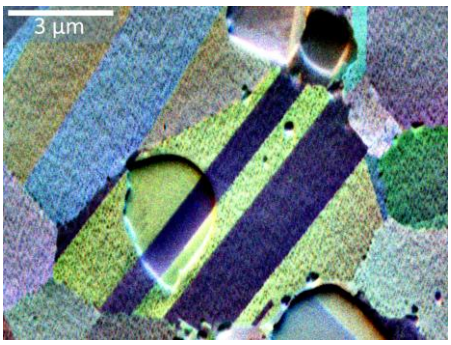

Introduction

René 65™ is a γ-γ' polycrystalline nickel based superalloy that has been derivated from the René 88™ PM alloy for allowing the casting and forging processing route (Heaney et al., 2014). γ-γ' Nickel-based superalloys are basically composed of a γ matrix (FCC solid solution) and second phase γ' precipitates adopting a $L1_2$ crystal structure. Depending on the alloy composition, the γ' phase mainly contains either Ni and Al elements (Ni_3Al) or Ni, Ti and Al ($Ni_3(Al,Ti)$). The γ' precipitates adopt a complex multimodal size distribution, following on from the thermomechanical processing route (Radis et al., 2008).

Large particles (round shaped, several micrometers large) formed at high temperature, are referred to as primary precipitates. They aim at pinning grain boundaries during hot processing below the γ' solvus temperature. The other precipitates are much smaller, one to two decades below in size, and intragranular. They typically form either during cooling after forging (Radis et al., 2008; Grosdidier et al., 1998), or during a dedicated thermal treatment designed for optimizing their distribution to improve in-service properties. The so-called

secondary precipitates form at first. A third class of tiny tertiary precipitates may then form in between the pre-existing ones, during subsequent cooling.

Studies dedicated to the coarsening of fine γ' precipitates during ageing treatments (Ricks et al., 1983; Grosdidier et al., 1998; Radis et al., 2008) have all shown the same sequence of evolution. Initially spherical and coherent, they become cuboïdal, tend to form cuboïdal arrays then dendrites, progressively losing their coherency with the matrix. There is a critical size at which coherency is lost, with a typical maximum value around 0.7 µm (Brown & Woolhouse, 1970). Large particles in Ni based superalloys are thus generally incoherent with the matrix. Speaking in terms of energetic considerations, coherency is lost when precipitates reach the critical size at which the low energy of the coherent interface can no longer balance the increasing contribution of elastic strain to the free energy of the system. Dislocations nucleate at the interface to accommodate the misfit stress. Interfacial dislocation density and consequently interphase misorientation increase with further increasing the precipitate size.

For a coherent precipitate, the constrained lattice mismatch can be expressed as a function of the constrained crystal lattice parameter of the precipitate $a_{\gamma'}$ and the crystal lattice parameter of the matrix (far from the interface) a_{γ} (Weatherly & Nicholson, 1968):

$$\epsilon = \frac{2(a_{\gamma'} - a_{\gamma})}{(a_{\gamma'} + a_{\gamma})} \quad (1)$$

Once the particle reaches the critical size for loosing coherency, the γ' recovers its unconstrained lattice parameter, as if it would be separated from the matrix. The corresponding unconstrained lattice mismatch δ is higher, still expressed by formula (1) but with the unconstrained value of the precipitate lattice parameter. The constrained mismatch ϵ can be linked to the unconstrained one δ as (Woolhouse & Brown, 1970):

$$\epsilon = \delta\left(\frac{1+\nu}{1+2K+\nu(1-4K)}\right) \quad (2)$$

where ν is the Poisson ratio of the precipitate and K is the ratio of the shear modulus of the matrix over the shear modulus of the precipitate.

This paper demonstrates the presence of primary γ' precipitates with a diameter of several micrometers that are nevertheless coherent with the surrounding matrix grain in the γ-γ' Nickel-based superalloy René 65™. This feature could be highlighted thanks to a judicious combination of several experimental techniques. To the authors' knowledge, such a feature is reported here for the first time. The physical background of that surprising configuration is discussed in terms of crystal lattice misfit.

Material and experimental setups

The studied material has been provided by the Safran-Snecma company. Its nominal composition and the composition measured by EDS are given in Table 1 (Heaney et al., 2014). It has undergone a hot forging sequence under thermo-mechanical conditions triggering dynamic recrystallization (temperature range: 1000°C to 1050°C, i.e. below 1111°C, the γ' solvus temperature (Bond et al., 2014), strain rate range: $0.01s^{-1}$ to $0.1s^{-1}$), followed by air cooling. Secondary and tertiary precipitates were dissolved at the processing temperatures and formed again upon cooling. They are out of the scope of this paper, which focuses on primary precipitates.

Element (wt%)	*Ni*	*Cr*	*Co*	*Ti*	*Al*	*Mo*	*W*	*Fe*	*Nb*
Nominal	Base	**16**	13.0	3.7	2.1	4.0	4.0	1	0.7
Measured (EDS)	54.2	**16.5**	13.3	4.7	2.0	3.6	4.2	1.0	0.4

Table 1: Nominal and measured compositions of the René 65 ™ alloy.

Combined EDS/EBSD analysis

Mirror polished samples were characterized using a combined EDS/EBSD (Energy Dispersive X-ray Spectrometry / Electron Back-Scattered Diffraction) fast acquisition speed system mounted on a high resolution Scanning Electron Microscope (SEM) (Zeiss Supra 40, equipped with a field emission gun (FEG)). The EDS/EBSD system is a QUANTAX system from the Bruker company, including an EDS XFlash 5030 detector and a e$^-$Flash^{HR} EBSD detector, controlled by the ESPRIT software package.

The γ phase is a FCC solid solution, which gives rise to the typical diffraction signals of crystallographic planes fulfilling the condition that Miller indices (h, k, l) are either all three even or all three odd. In other words, the planes for which Miller indices have different parity lead to a so-called systematic extinction, because their structure factor and therefore the diffracted intensity are then equal to zero. The γ' precipitates have an ordered structure, which is simple cubic. Thus, the former systematic extinction criterion does not apply any longer. Crystallographic planes with both odd and even Miller indices can diffract, but only weak intensities (few percents only of the intensities diffracted by planes with all three Miller indices of the same parity). Moreover, as shown below, the lattice parameters of both γ and γ' phases are close to each other. Distinguishing those phases based on EBSD patterns may therefore only be based on the presence/absence of very low intensity diffraction signal, which by itself is not trivial under EBSD settings optimized for orientation mapping. In addition, intragranular (secondary and tertiary) precipitates are generally present inside the matrix, have the same orientation as the matrix, and are too small to be spatially resolved. As a consequence the matrix diffraction patterns also exhibit weak diffracted intensities instead of no intensity at all for the planes corresponding to the systematic extinctions. From a practical point of view, EBSD is thus unable to distinguish γ and γ' phases in Ni based superalloys. The straightest way to overcome this is to use EDS combined with EBSD, in order to discriminate phases based on their chemical composition.

EDS has typical spatial resolution of about 1 μm, which is far above the few tens of nm achievable with EBSD; but this limitation will not be detrimental in the present study focused on the large primary precipitates. In order to improve the EDS spatial resolution at best while still exiting the characteristic X-rays of interest and preserving the quality of the Kikuchi diagrams, the accelerating voltage of the electron beam has been settled to 15 kV. Combined EDS-EBSD maps were acquired with a step size of 46 nm, at the speed of 70 points per second.

For complementary and finer scale TEM analyses, thin foils were prepared by double face mirror polishing down to a thickness of 100 μm. 3mm disks were cut out from the thin foil and their thickness was further reduced using a dimpler. Electron transparency was finally achieved by ion milling using a Precision Ion Polishing System (PIPS) Gatan 691 with a 6 kV acceleration voltage and with an ion beam incidence angle of 6°. TEM and STEM observations were conducted on a JEOL 2100 Field Emission Gun TEM operated at 200 kV and equipped with an Ultra-thin window JEOL EDS detector.

In addition, the lattice mismatch was measured using X-ray diffractograms recorded within the θ-2θ setup on a mirror polished (5 mm x 5 mm) sample. The wavelength of X-ray beam was that of the Cu-Kα radiation, 0.15418 nm. A Xpert'Pro MTD diffractometer and a PIXcel

(PAN analytical) detector were used, covering angles from 20 to 50 degrees, with a total time exposure of 4 hours and 30 minutes.

Results

EDS spectra were acquired in the SEM and analyzed following the default settings of the software, without using a standard for improving the quantification accuracy. The obtained overall composition, given in Table 1, is nevertheless in good agreement with the nominal values. The EDS elemental maps obtained by SEM (Fig.1) and the corresponding chemical composition of the γ and γ' phases given in Table 2 show that Chromium and Cobalt are segregated in the matrix while the inverse tendency is observed for Titanium and Aluminum. The smallest precipitates resolved are about half a micrometer in diameter.

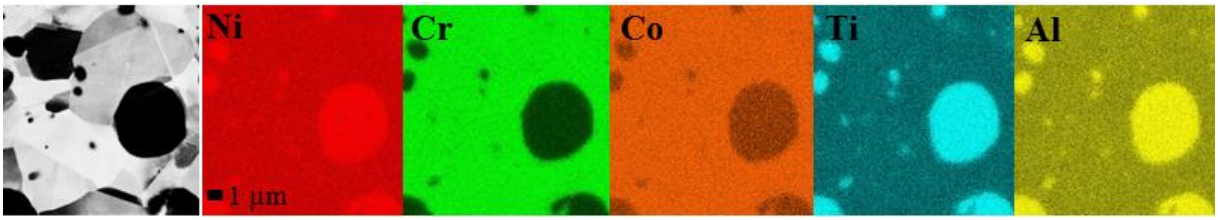

Figure 1 : Back-scattered electron image and EDS maps of the main alloying elements in René 65 ™.

Element (wt%)	*Ni*	*Cr*	*Co*	*Ti*	*Al*	*Mo*	*W*	*Fe*	*Nb*
Matrix γ	54.9	**17.9**	**14.3**	3.6	1.6	3.6	2.9	0.9	0.3
Primary γ' precipitates	69.7	3.1	7.7	**11.1**	**5.3**	0.7	1.0	0.2	1.2

Table 2: Composition of the René 65™ phases (measured by EDS).

The relative concentration of Cr and Ti has been chosen as a criterion for attributing a phase to each measurement point. A combined EDS/EBSD dataset contains, for each measurement point (or map pixel), the x and y coordinates of the point, the position of the Hough transform peaks and the complete EDS spectrum. During post-processing, the amount of Cr and Ti of the EDS spectrum of a given pixel is compared to reference compositions of both phases and the pixel is assigned to one of them. Those reference spectra were acquired by measuring the composition in the center of a large matrix grain containing no intragranular γ' particles; and in the middle of a large primary γ' precipitate. Several spectra have been averaged for building the reference composition of each phase. Within the combined EDS/EBSD setup, composition thresholds are set so that, if the EDS spectrum deviates a little from the γ' reference, it will be assigned as γ phase. It occurs at the rim of the precipitates, where the matrix has a contribution to the spectrum due to the limited spatial resolution of the EDS technique (the precipitates are a bit smaller as detected by the EDS-EBSD method as compared to their size in the BSE images). Based on this semi-quantitative analysis, primary and large secondary γ' precipitates can be discriminated from γ matrix.

The same area of the microstructure of a forged sample of René 65™ has been analysed using the coupled EDS/EBSD technique (Figs. 2b-d) and imaged using a back-scattered electrons

(BSE) detector (Fig. 2a). On the latter, the γ' precipitates appear as darker areas, because of their lower average atomic number as compared to the one of the γ matrix.

First of all, the comparison between Figs. 2a and 2b shows that the localization and shape of precipitates on the phase map corresponds well to the precipitates revealed by the BSE image. The EDS/EBSD coupling method described above is thus proved to be relevant for identifying primary precipitates. On Fig. 2b, the simultaneous representation of phases and grain boundaries shows that some primary γ' precipitates are located inside γ grains. Since they are supposed to pin boundaries during thermomechanical processing, they are usually expected to be on grain boundaries or at triple junctions. Three typical examples of intragranular primary γ' precipitates are arrowed on Fig. 2b. One important characteristic of this configuration is that only one precipitate is contained per matrix grain.

The comparison between the phase map of Fig. 2b and the orientation color-coded map of Fig. 2c reveals a specific orientation relationship between those precipitates and their surrounding matrix grain. Invisible on Fig. 2c, they have obviously the same orientation as the surrounding grain, within the EBSD angular resolution (typically 0.5°). Fig. 2d is colored according to the Kernel Average Misorientation (KAM) value. The KAM parameter is efficient for revealing subboundaries and interfaces with very low misorientation angles. Here, the trace of γ' precipitates inside matrix grains is hardly visible on the KAM map. In those coherent precipitates, even defects such as annealing twins are extended to the matrix grain. The main KAM contrast arises either from differences in the orientation of the grains themselves which lead to slight variations in the pattern indexation accuracy, or from lattice distorsions associated with the presence of dislocations in few unrecrystallized grains (e.g. the one at the bottom right).

On the other hand, it is worth mentioning that there also exist incoherent primary precipitates, which are separated from the matrix by high angle boundaries. They are located at grain boundaries and have no specific orientation relationship with their neighbor matrix grains. Manual counting of 1400 precipitates on BSE images led to the conclusion that 52% of the primary precipitates were coherent with their surrounding grain.

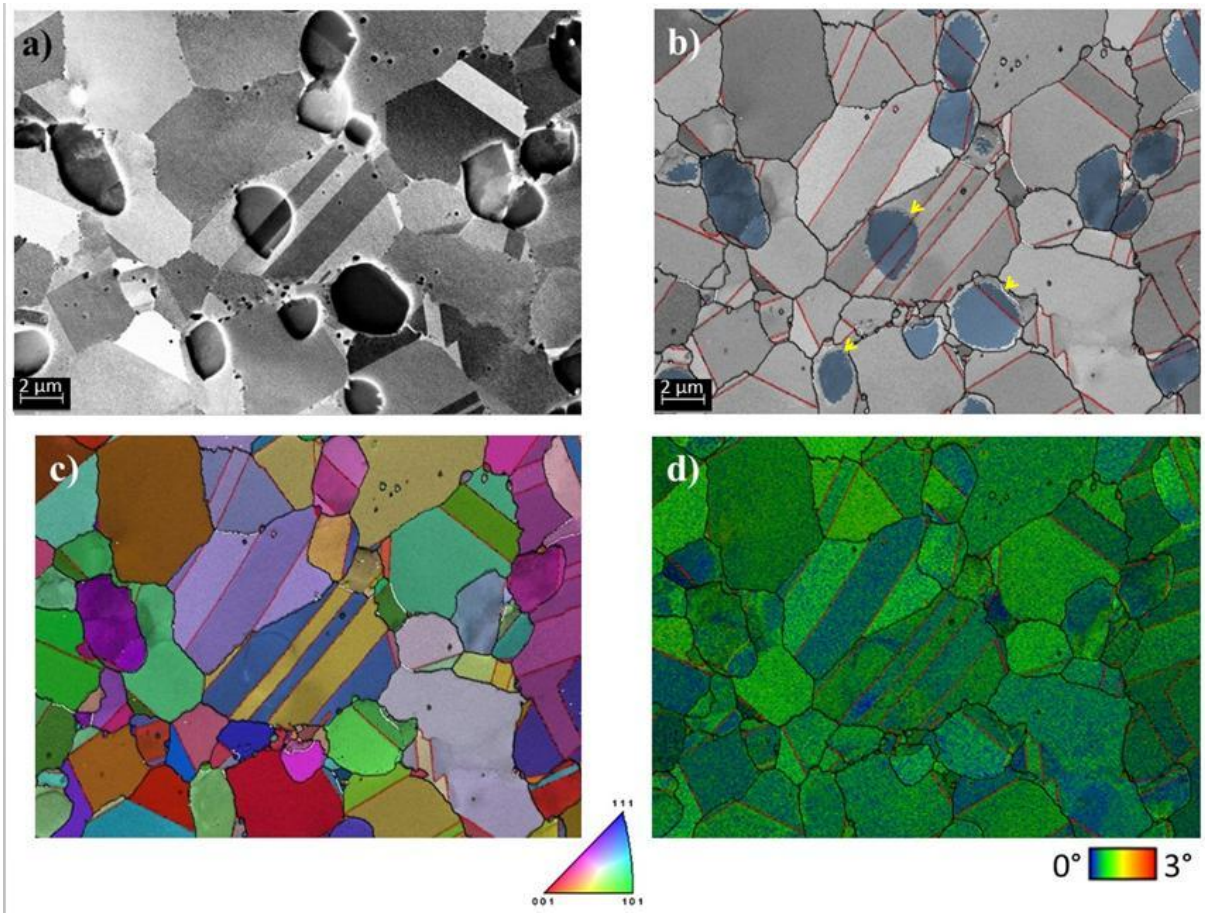

Figure 2: Microstructure of the as-received René 65™ sample. a) BSE image. b) γ' phase map (in light blue) obtained from post-processing of EDS/DEBSD data, superimposed on the Kikuchi Pattern Quality map. c) Orientation color coded map (normal direction to the scanned section projected into the standard triangle) of both phases superimposed on the Kikuchi Pattern Quality map. d) Kernel Average Misorientation map (average misorientation angle between each pixel and its first neighbors, excluding disorientations higher than 3°). On b), c) and d) low angle grain boundaries (3-10°) are drawn white, high angle grain boundaries black (>10°) and twins (60° around <111> with a tolerance of 5°) in red.

The coherency of large intragranular γ' precipitates was further investigated at a finer scale by TEM. Fig. 3a shows a STEM bright field image of a large primary precipitate surrounded by a matrix grain, as confirmed by the EDS elemental maps of Fig. 3c. The diffraction patterns of selected areas corresponding to either the precipitate or its surrounding grain evidence their coherency. The diffraction pattern corresponding to the matrix (Fig. 3b1) is typical from a FCC crystal structure within a [011] zone axis, with characteristic systematic extinctions. On the contrary, additional spots corresponding to (h, k, l) Miller indexes of mixed parity are visible on the diffraction pattern of the precipitate (Fig. 3b2). A thin twin lamella (arrowed) is crossing the entire precipitate and extends inside the γ matrix grain.

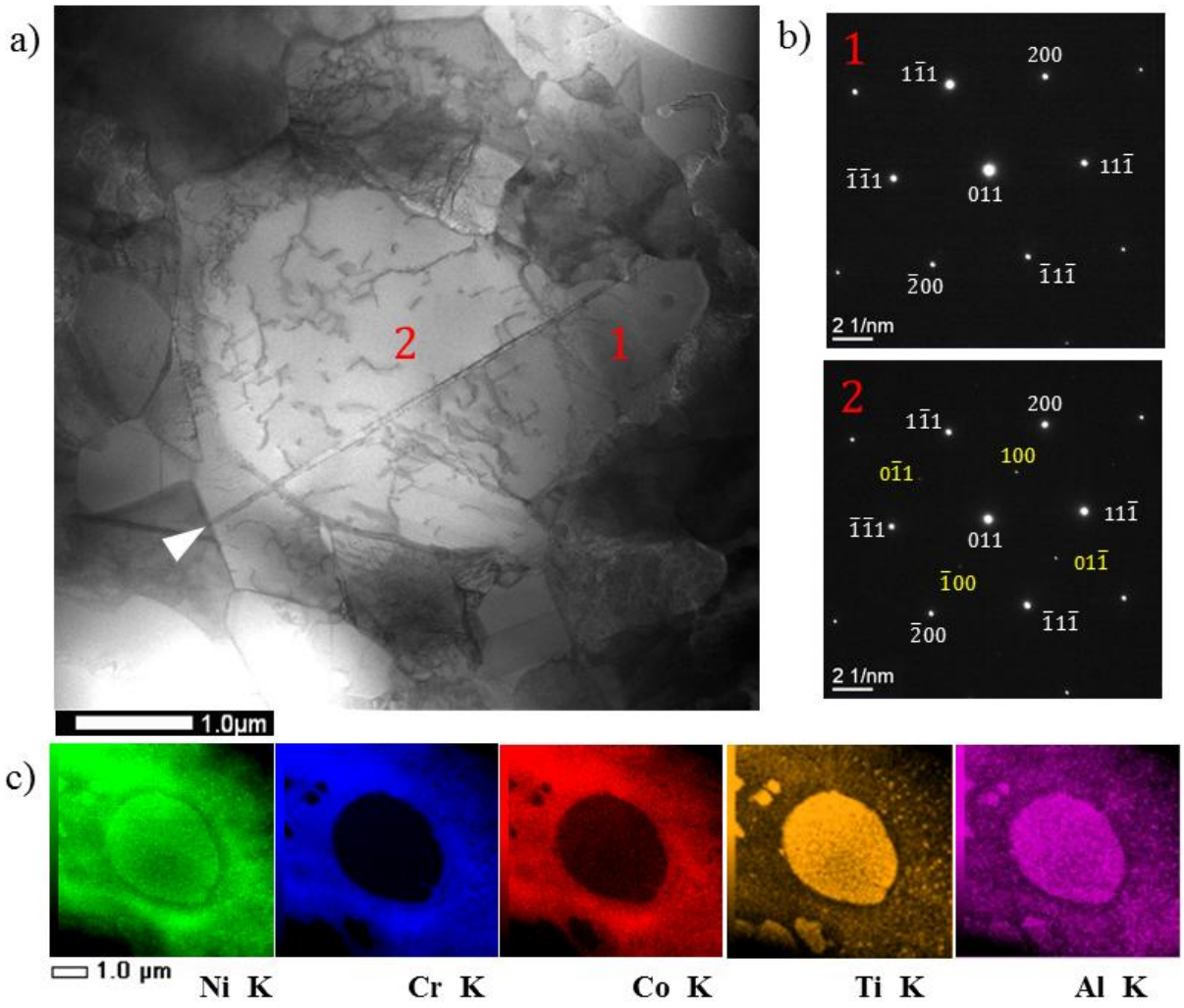

Figure 3: a) STEM image of a primary precipitate surrounded by a γ grain. b) Selected area diffraction patterns in [110] zone axis, corresponding to the γ grain (1) and the γ' precipitate (2). c) EDS maps of the main chemical elements.

A High-Resolution TEM image taken at the interphase is shown on Fig. 4. Although the interface is not clearly depicted, Fast Fourier Transforms simulating diffraction patterns confirm the area A to be γ', and area B to be γ phase. The absence of a clear transition along the length of the image suggests that phases have very close values of lattice parameter, even though the lattice mismatch could not be accurately measured using this technique. No dislocation could be detected on that image, suggesting that the interphase dislocation density is low enough that some areas are defect free. Further investigations are necessary to quantify the interface dislocation density, but it can be inferred from the preliminary results shown here that it is likely to be low.

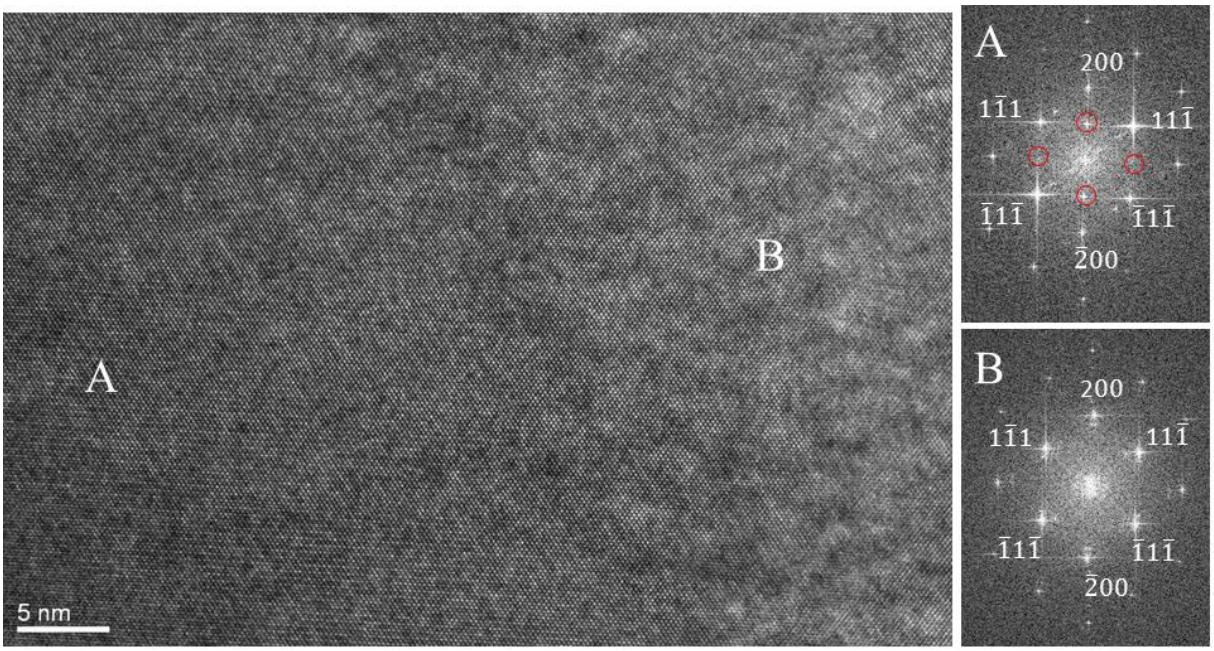

Figure 4: High-resolution Transmission Electron Microscopy (HRTEM) in bright field, at the interface of coherent y and y' structure; with corresponding diffraction patterns simulated by Fast-Fourier Transformations.

In order to determine the value and sign of the lattice mismatch at room temperature, X-ray measurements were conducted. The $(011)_{\gamma'}$ and $(111)_{\gamma}$ fundamental reflections respectively led to lattice parameters values of 0.361 ± 0.001 nm for $a_{\gamma'}$ and 0.360 ± 0.001 nm for a_{γ}.

Discussion

The EDS/EBSD coupling technique has enabled to reveal an unusual γ-γ' configuration in a hot-forged recrystallized microstructure of René 65^{TM} alloy. About half of the large primary γ' precipitates are surrounded by a matrix grain with the same crystallographic orientation. This was confirmed by complementary TEM observations. While the secondary and tertiary precipitates are generally coherent with their hosting grain, such configuration has not been reported yet for primary precipitates.
Studies dedicated to the evolution of growing γ' particles during ageing treatments (Ricks et al., 1983; Nathal et al., 1985) have shown that the critical size at which the particles become incoherent depends on the γ-γ' lattice mismatch. In the case of a very low constrained lattice mismatch (typically $|\epsilon| < 0.05\%$), growing precipitates can remain coherent until they reach a diameter of 0.5-0.7 µm (Ricks et al., 1983; Radis et al., 2008).

The lattice mismatch at room temperature is too low to be measured by XRD, both phases appear to have lattice parameters with overlapping uncertainty ranges. From those values, the lattice mismatch ε can only be estimated to be below 0.8%. The constrained lattice mismatch of similar alloys is well documented in the literature. Alloys such as IN 100, RR2000, MAR M 002 DS, SRR 99, exhibit lattice misfits at room temperature of 0.65%, 0.79%, 0.55% and 0.59% respectively (Tawancy et al., 1994). The Nimonics group possesses lower misfits:

Nimonic 115: -0.18%, Nimonic 90: 0.34%. Finally, Nimonic 105 and Udimet can be distinguished, their lattice misfit almost reaching the zero-value: 0.03% (Ecob et al., 1982) or -0.04% for Nimonics 105 and $\epsilon < 0.02\%$ in Udimet 720 (Ricks et al., 1983). René 65™ belongs to the last group, as well as the powder metallurgy René 88DT from which it has been derived. René 65 and René 88 alloys have very close chemical compositions and the lattice mismatch of René 88DT has indeed been already settled as especially low, with a constrained lattice mismatch around or below 0.05% to 0.06% (Wlodek et al., 1996; Srinivasan et al., 2009). Such extremely low values are in agreement with the results obtained from our XRD measurements.

Since the observed microstructure has developed during processing at high temperature, the effect of thermal expansion must be taken into account. Grose and Ansell (1981) and Nathal et al. (1985) have emphasized the temperature dependence of the lattice mismatch in various γ-γ' alloys, in the range of 25°C to 1000°C and showed that the matrix expands to a greater extent than the γ' precipitates. As a consequence, alloys exhibiting a low but positive lattice mismatch at room temperature may reach a close-to-zero, or even negative, lattice misfit at higher temperatures.

For supporting the existence of multimicrometric coherent precipitates, the lattice misfit must be close to zero (a rough estimation of the constrained mismatch allowing such large coherent structures, by balancing the contributions of the interfacial energy and the elastic strain energy, leads to $\epsilon = 0.03\%$ for 5 µm coherent precipitates), which is consistent with the very low positive value measured at room temperature in the René 65™ alloy, and with the lattice misfit tending to decrease with increasing temperature. Even though, the lattice misfit may not be the factor triggering the formation of the observed coherent structures during forging of René 65™, its contribution appears to be essential for allowing their stability.

Further investigations are required for determining the formation mechanisms: does the precipitate grow coherently in the hosting grain up to the observed sizes, or does the surrounding grain develop coherently around a pre-existing primary precipitate by some specific recrystallization mechanism? Works are currently being done by the authors, with results clearly in favor of the second hypothesis, as will be detailed in a following paper.

Conclusions

1. EDS/EBSD coupling has proved to be a suitable tool for discriminating γ and γ' phases in the René 65™ alloy. It enables to study simultaneously the phase topology as well as the possible orientation relationships, with a spatial resolution of the γ' precipitates of about 0.5 µm under the applied experimental conditions.
2. In the studied forged material, about half of the primary precipitates appeared to be intragranular and coherent with their surrounding matrix grain. In those large coherent precipitates, twins are extended from one phase to the other. The other half is made of incoherent particles with similar sizes, but located on grain boundaries and triple junctions.
3. A close-to-zero lattice mismatch is a key factor for the stability of such wide γ-γ' coherent interfaces. The lattice mismatch could indeed be evaluated as lower than 0.3% at room temperature, and is known to decrease with increasing temperature.
4. The metallurgical mechanisms from which those configurations originate have to be investigated, as well as their impact on microstructure evolution during thermomechanical processing.

5. Since other Nickel based superalloys have similar lattice mismatch values, it would be worth re-analyzing them using the combined EDS/EBSD technique employed here, to seek for the presence of such large coherent particles.

Acknowledgements

The authors would like to thank the Snecma-SAFRAN company, for their financial support; the CEMEF technical staff members, Suzanne Jacomet for her support in SEM investigations and Gabriel Monge for the X-rays measurements; and Daniel Galy from the Synergie4 company for his help in the EDS/EBSD setup configuration.

References

Bond, B.J. et al., 2014. René 65 Billet Material for Forged Turbine Components. In U. John Wiley & sons, Inc., Hoboken, NJ, ed. *8th International Symposium on Superalloys718 and Derivatives*. pp. 107–118.

Brown, L.M. & Woolhouse, G.R., 1970. The loss of coherency of precipitates and the generation of dislocations. *Philosophical Magazine*, 21(170), pp.329–345.

Ecob, R.C., Ricks, R.A. & Porter, A.J., 1982. The measurement of precipitate/matrix lattice mismatch in nickel-base superalloys. *Scripta Metallurgica*, 16(9), pp.1085–1090.

Grosdidier, T., Hazotte, A. & Simon, A., 1998. Precipitation and dissolution processes in γ/γ′ single crystal nickel-based superalloys. *Materials Science and Engineering: A*, 256(1-2), pp.183–196.

Heaney, C.M. et al., 2014. Development of a New Cast and Wrought Alloy (René 65) for High Temperature Disk Applications. In U. John Wiley & Sons, ed. *8th International Symposium on Superalloy 718 and Derivatives*. pp. 67–77.

Nathal, M.V., Mackay, R.A. & Garlick, R.G., 1985. Temperature dependence of γ-γ' lattice mismatch in Nickel-base superalloys. *Materials Science and Engineering*, 75(1-2), pp.195–205.

Radis, R. et al., 2008. Evolution of size and morphology of gamma ' precipitates in UDIMET 720 Li during continuous cooling. *SUPERALLOYS 2008*, pp.829–836.

Ricks, R.A., Porter, A.J. & Ecob, R.C., 1983. The growth of γ′ precipitates in nickel-base superalloys. *Acta Metallurgica*, 31(1), pp.43–53.

Srinivasan, R. et al., 2009. Atomic Scale Structure and Chemical Composition across Order-Disorder Interfaces. *Physical Review Letters*, 102(8), p.086101.

Tawancy, H.M. et al., 1994. Thermal stability of advanced Ni-base superalloys. *Journal of Materials Science*, 29 (9), pp.2445–2458.

Weatherly, G.C. & Nicholson, R.B., 1968. An electron microscope investigation of the

interfacial structure of semi-coherent precipitates. *Philosophical Magazine*, 17(148), pp.801–831.

Wlodek, S., Kelly, M. & Alden, D., 1996. The structure of Rene 88 DT. *SUPERALLOYS 1996*, pp.129–136.

Woolhouse, G. & Brown, L., 1970. Studies of coherency in internally oxidized copper alloys. *Journal of the Institute of Metals*, 98, p.106.